4-1-2008

A quantitative assessment of empirical magnetic field models at geosynchronous orbit during magnetic storms

Chia-Lin L. Huang
hcl@guero.sr.unh.edu

Harlan E. Spence
Boston University, harlan.spence@unh.edu

H. J. Singer

N. A. Tsyganenko

Recommended Citation
Huang, C.-L., H. E. Spence, H. J. Singer, and N. A. Tsyganenko (2008), A quantitative assessment of empirical magnetic field models at geosynchronous orbit during magnetic storms, J. Geophys. Res., 113, A04208, doi:10.1029/2007JA012623.

A quantitative assessment of empirical magnetic field models at geosynchronous orbit during magnetic storms

A quantitative assessment of empirical magnetic field models at geosynchronous orbit during magnetic storms

Chia-Lin Huang,[1] Harlan E. Spence,[1] Howard J. Singer,[2] and Nikolai A. Tsyganenko[3]

Received 2 July 2007; revised 13 November 2007; accepted 20 December 2007; published 11 April 2008.

[1] We evaluate the performance of recent empirical magnetic field models (Tsyganenko, 1996, 2002a, 2002b; Tsyganenko and Sitnov, 2005, hereafter referred to as T96, T02 and TS05, respectively) during magnetic storm times including both pre- and post-storm intervals. The model outputs are compared with GOES observations of the magnetic field at geosynchronous orbit. In the case of a major magnetic storm, the T96 and T02 models predict anomalously strong negative B_z at geostationary orbit on the nightside due to input values exceeding the model limits, whereas a comprehensive magnetic field data survey using GOES does not support that prediction. On the basis of additional comparisons using 52 storm events, we discuss the strengths and limitations of each model. Furthermore, we quantify the performance of individual models at predicting geostationary magnetic fields as a function of local time, D_{st}, and storm phase. Compared to the earlier models (T96 and T02), the most recent storm-time model (TS05) has the best overall performance across the entire range of local times, storm levels, and storm phases at geostationary orbit. The field residuals between TS05 and GOES are small ($\leq$3 nT) compared to the intrinsic short time-scale magnetic variability of the geostationary environment even during non-storm conditions ($\sim$24 nT). Finally, we demonstrate how field model errors may affect radiation belt studies when estimating electron phase space density.

Citation: Huang, C.-L., H. E. Spence, H. J. Singer, and N. A. Tsyganenko (2008), A quantitative assessment of empirical magnetic field models at geosynchronous orbit during magnetic storms, *J. Geophys. Res.*, *113*, A04208, doi:10.1029/2007JA012623.

1. Introduction

[2] Earth's magnetic environment has been measured nearly continuously in space for more than four decades, making it possible to model its average configuration for different levels of geomagnetic activity. More than a dozen major empirical magnetic field models have been developed since the beginning of the space era [e.g., *Hones*, 1963; *Mead*, 1964; *Taylor and Hones*, 1965; *Williams and Mead*, 1965; *Olson and Pfitzer*, 1974, 1977; *Mead and Fairfield*, 1975; *Tsyganenko and Usmanov*, 1982; *Tsyganenko*, 1987, 1989, 1995, 1996, 2002a, 2002b; *Tsyganenko et al.*, 2003; *Tsyganenko and Sitnov*, 2005]. These models are valuable, for instance, for studies assessing magnetic connectivity between different regions in the magnetosphere, for correlating spacecraft measurements with ground-based observations, and for providing global magnetic fields needed for energetic particle drift motion studies, e.g., *Ukhorskiy et al.* [2006]. Finally, they are also used for validating global MHD simulations of the magnetosphere to establish confidence in the global MHD results [*Pulkkinen et al.*, 1995; *Huang et al.*, 2006]. In all the above studies, accurate model predictions are critically important, since inaccurate field predictions could fundamentally alter scientific conclusions. Hence quantifying the strengths and limitations of empirical magnetic field models benefits both model users and developers.

[3] Previous tests and evaluations of empirical models have used a variety of approaches [e.g., *Walker*, 1976; *Spence et al.*, 1987; *Peredo et al.*, 1993; *Stern*, 1994; *Reeves et al.*, 1996; *Thomsen et al.*, 1996; *Pulkkinen and Tsyganenko*, 1996]. However, a decade has passed since the last objective analysis of empirical magnetic field models. During that period, newer empirical models were developed, based on larger data sets and more sophisticated methods. Physically more relevant input parameters were used to quantify the impact of the upstream solar wind and IMF conditions on the magnetosphere, and also its dependence on the concurrent D_{st} index. A more advanced parameterization has also been introduced, including the effect of nonlinear saturation of magnetospheric currents during periods with extremely strong interplanetary driving. However, those models have not yet undergone a thorough testing based on independent data. Given the fact that extreme conditions are quite rare, it remains an open question to what extent can users trust the model output in the case of strong storms. The goal of the present paper is to fill that gap by providing a comprehensive test of the

[1]Center for Space Physics, Boston University, Boston, Massachusetts, USA.
[2]Space Weather Prediction Center, NOAA, Boulder, Colorado, USA.
[3]Department of Terrestrial Physics, University of Saint-Petersburg, Petrodvorets, Saint-Petersburg, Russian Federation.

0148-0227/08/2007JA012623

Table 1. Summary of the Distinguishing Properties of the Tsyganenko Models (T96, T02, and TS05): Boundary Prescriptions, Field Sources, Fitted Magnetic Field Data, Model Inputs, and Calculation Methods

	T96	T02	TS05
Boundary prescriptions	magnetopause based on *Sibeck et al.* [1991]	magnetopause based on *Shue et al.* [1998] and tailward $\leq 15\ R_E$	same as T02
Field sources	$B_{CF} + B_{SRC} + B_{TC} + B_{FAC} + B_{INT}$	same as T96, plus B_{PRC}	same as T02
Fitted magnetic field data	non-storm and stormtime data[a]	same as T96[b]	storm-time data from 37 magnetic storm events[c]
Model inputs	P_{dyn}, D_{st}, IMF B_y and B_z and dipole tilt	same as T96, plus two indices (G_1 and G_2) representing time-integration effect	same as T96, plus six indices ($W_1 - W_6$) representing time-integration effect
Calculation methods	linear amplitude of the field sources depends on model inputs	same as T96	non-linear saturation for extreme storm conditions; each field source has its own relaxation time and driving functions

[a]IMPs, HEOS, ISEE-1 and 2.
[b]Geotail, Polar, ISEE-2, AMPTE/CCE, AMPTE/IRM, CRRES, and DE-1.
[c]GOES-8, 9, and 10, Polar, Geotail, and Equator-S.

above models, using a large independent set of geosynchronous data.

[4] In this paper, we evaluate the three most recent Tsyganenko models (T96, T02 and TS05) by comparing the model results with satellite measurements, and we discuss and quantify improvements relative to earlier versions. Geosynchronous orbit represents the transition region between Earth's internal dipole field and the externally produced field of the outer magnetosphere. Large gradients across this region and its comparable proximity to major external field sources make it an especially sensitive location for assessing both global current structures and their dynamics. With the above in mind, we compare the model outputs with magnetic field observations by GOES satellites for various geomagnetic activity levels. We perform a case study analysis of a major magnetic storm to quantify strengths and weaknesses of model predictions. In particular, T96 and T02 models predict strong negative B_z (in GSM coordinates) fields at geostationary orbit near local midnight during storms, but such fields are not substantiated by the results of a GOES data survey. Finally, we evaluate the recent Tsyganenko models (T96, T02, and TS05) during a collection of 52 individual geomagnetic storms. This statistical study quantifies the limitations and accuracy of the models over a broad range of local times, activity levels, and storm phases, including pre- and post-storm.

2. Description and Comparison of Recent Tsyganenko Models

[5] Tsyganenko magnetic field models are empirical and global, based on a very large number of satellite magnetic field measurements collected throughout the magnetosphere over the past three decades. The models produce global, parameterized, quasi-static states of Earth's dynamic magnetospheric configurations. Tsyganenko models use physically based functional forms to describe the electrical current systems responsible for the external field; the internal main field is the International Geomagnetic Reference Field (IGRF, http://www.ngdc.noaa.gov/IAGA/vmod/igrf.html). Table 1 summarizes the distinguishing properties of the most recent Tsyganenko models: boundary prescriptions, field sources, fitted magnetic field data, model inputs, and methods. In the following, we introduce the basic properties of the three models and describe the major differences between them. For more detailed model information, please see *Tsyganenko* [1996, 2002a, 2002b] and *Tsyganenko and Sitnov* [2005] for T96, T02, and TS05, respectively.

2.1. Tsyganenko 1996 Model

[6] The spatial boundary of T96 is a hemi-ellipsoid on the dayside, which merges in the magnetotail with a cylindrical surface based on the average magnetopause of *Sibeck et al.* [1991]. The model field is the sum of five physically different vector magnetic fields, including contributions from the Chapman-Ferraro current (B_{CF}), symmetric ring current (B_{SRC}), cross-tail current sheet (B_{TC}), large-scale field-aligned currents (B_{FAC}), and partial penetration of the IMF into the model magnetosphere (B_{INT}). The magnetospheric magnetic field data include measurements from IMP, HEOS, and ISEE satellites. The model inputs are the upstream solar wind dynamic pressure, IMF B_y and B_z, D_{st}, and dipole tilt angle. Each field source is a function of location and model input parameters, with the function coefficients determined by fitting to the data. T96 uses a directional least squares fitting criterion to derive the model field from spacecraft data. Valid model input ranges are: Solar wind dynamic pressure between 0.5 and 10 nPa, D_{st} between -100 and $+20$ nT, and IMF B_y and B_z between -10 and $+10$ nT.

2.2. Tsyganenko 2002 Model

[7] T02 is based on a different set of data that focuses on the inner magnetosphere: the magnetic field data set

includes observations from Polar, Geotail, ISEE, AMPTE, CRRES, and DE-1 satellites. The model field is confined within a dynamical magnetopause, based on the empirical model of *Shue et al.* [1998]; on the nightside its region of validity is limited to tailward distances $\leq$15 R_E. T02 ring current includes not only a symmetric component but also a partial ring current (B_{PRC}) with field-aligned closure currents. This improvement makes it possible to represent local time asymmetries of the inner magnetospheric field, which is particularly important during the storm main phase. The model inputs for T02 are similar to T96, except that the former has two extra indices (G_1 and G_2) to capture the time history driving of the magnetosphere by the solar wind. The time-integrated indices are based on the average solar wind and IMF data over the 1-hour interval preceding the current observations of the magnetospheric field. The coefficient determination of T02 is similar to that of T96, but uses a standard merit function, equal to the root-mean square deviation of the model external field from the observed one.

2.3. Tsyganenko and Sitnov 2005 Storm Model

[8] TS05 was specifically developed to reproduce the storm-time magnetosphere within a similar spatial region as that covered by T02. It is parameterized by dynamical solar wind inputs and includes a non-linear saturation of the field sources for strong solar wind conditions. The magnetic field data set for this model comprised 37 storm events that occurred between 1996 and 2000 and were observed by GOES, Polar, Geotail, and Equator-S satellites. TS05 has six input parameters (W_1–W_6), defining the strengths of individual field sources, similar to the time-integrated indices of T02; each parameter quantifies the combined effect of the interplanetary driving of the magnetospheric currents and their relaxation toward an unperturbed state.

3. Case Study: Model-Predicted Strong $-B_z$ Near GOES Local Midnight

[9] First, we compare model predictions with GOES observations during a major geomagnetic storm associated with a magnetic cloud. Throughout the storm period (24–26 September, 1998, noted as Sep98 event hereafter), the Wind satellite continuously measured the solar wind and IMF data at 180 R_E upstream. Figure 1a shows the D_{st} index for 25 September. A prolonged southward IMF lasting for 12 hours, created a large magnetic field disturbance and a D_{st} minimum of −213 nT. Figure 1b compares the GOES-8 magnetic field (GSM B_z component) data and Tsyganenko model outputs. The black line is the magnetic field as measured by GOES-8, corrected for the known ∼7 nT offset from the Z component in spacecraft coordinates according to *Tsyganenko et al.* [2003]. The colored lines are the predictions of the three models (T96 in green, T02 in blue, and TS05 in red) at GOES-8's position, using time-dependent upstream solar wind inputs from the Wind satellite. We show only the Z component of the fields because it exhibits the largest difference between the measurements and model results; the X and Y differences are much smaller and not strongly model dependent.

[10] From the three models analyzed, TS05 yields the best result in reproducing the overall trend of the GOES-8 magnetic field throughout the storm event. During 0 to 12 UT on 25 September, T96 and T02 predict negative B_z (minimum values: −45 and −90 nT, respectively) at geostationary orbit when near local midnight (5 UT ∼0 LT for GOES-8). These anomalously strong negative B_z values (noted as $-B_z$ hereafter) are inconsistent with the small $-B_z$ fields (−10 nT) observed by GOES over a short period of time at 4 UT. To investigate the cause of the anomalous $-B_z$ predictions, we explore the different models' vector magnetic field sources.

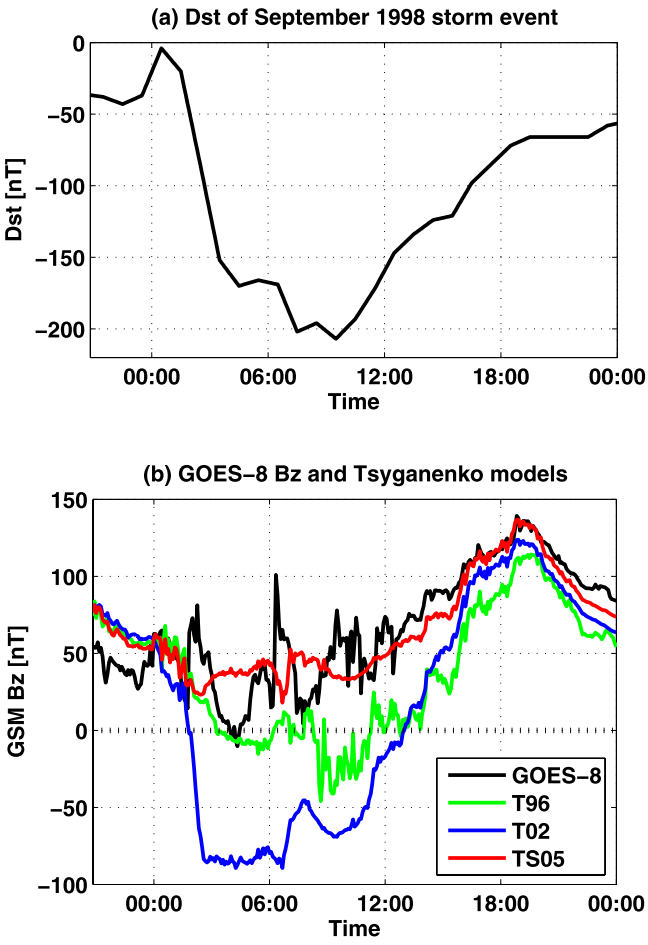

Figure 1. D_{st} and geostationary magnetic field during a major storm on 25 September 1998 in universal time. Panel (b) shows the GOES-8 GSM B_z magnetic field (in black) and the Tsyganenko model predictions at GOES-8's position (T96 in green, T02 in blue, and TS05 in red). The predicted B_z value include the IGRF and the model external field.

[11] The relative contributions of the field sources in each model are very different throughout the storm event. The tail and ring currents are the primary contributors to the external field of T96 during storm main and recovery phases, respectively. Their sum over-estimates the $-B_z$ at geostationary orbit. For T02, the field source from the tail current dominates. The large and uncompensated tail current is the main reason for the anomalous predictions of strong $-B_z$ values on the nightside. In contrast, the TS05 external field sources, particularly the more flexible ring and

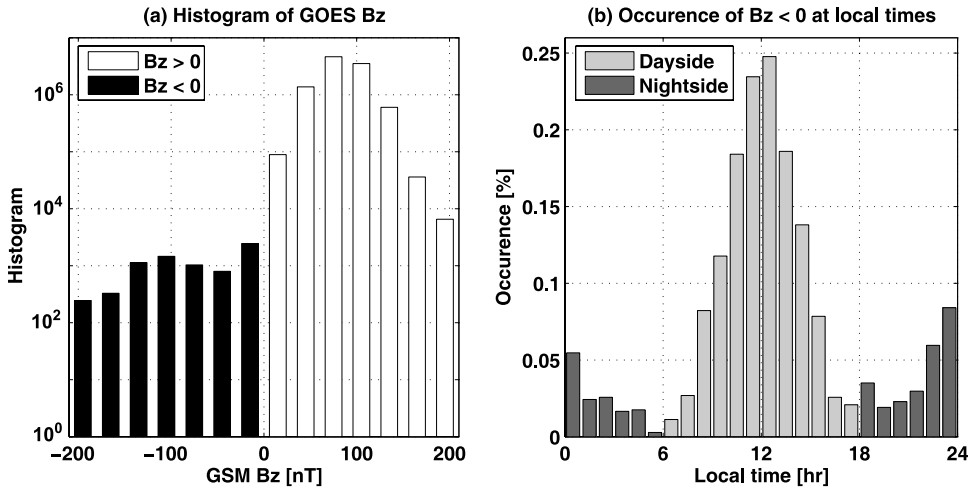

Figure 2. Results of GOES data survey searching for strong $-B_z$ near midnight: (a) logarithmic histogram of B_z values sorted by field magnitude; (b) percentage occurrence of $-B_z$ measurements at all local times. The average value of the nightside $-B_z$ fields (-7 nT) is much smaller than the average GOES B_z value at midnight (+66 nT).

tail currents, better represent theses currents and improve the model predictions.

[12] As noted earlier, GOES observes weak $-B_z$ fields on the nightside during the storm main phase. To assess whether the observed $-B_z$ is a large and persistent characteristic of geomagnetic storms and thus an important feature to reproduce, we perform a statistical data survey.

4. GOES Data Survey: Observed Weak $-B_z$ Near Local Midnight

[13] The GOES data survey includes 10 million magnetic field data points (1-min time resolution) from four GOES satellites (8, 9, 10, and 12) between 1996 and 2006. We collect the GOES data along with local time and D_{st} information and search for events that have large $-B_z$ measurements near GOES local midnight like the earlier models predict. The data survey starts by extracting the $-B_z$ measurements from the data set. Figure 2a shows a logarithmic histogram of all B_z data points sorted by field magnitude. The positive B_z values are in white bars, and the negative values are in black. Negative B_z occurs only 0.07% of the time. On the basis of this small occurrence rate, the magnetic field models are not likely to reproduce the rarely occurring $-B_z$ observed by GOES at geosynchronous orbit.

[14] To explore the source(s) of $-B_z$ observed at GOES in regions otherwise dominated by the dipole field, we first sort all $-B_z$ data points to find their local time dependence. Figure 2b shows the percentage occurrence of $-B_z$ data for all local times with respect to the total number of data points in each local time bin. The occurrence peak on the dayside ($7-17$ LT, light gray bars) comprises 78% of all $-B_z$ measurements. Such occurrences are likely the result of magnetopause crossings. The dayside $-B_z$ values are large as could be expected when satellites move into the field-compressed magnetosheath during periods of southward IMF. However, the $-B_z$ events observed on the nightside (± 6 h from 0 LT, dark gray bars) have relatively weak values (average -7 nT), compared to the normal strong positive GOES B_z values at midnight (average +66 nT).

[15] To understand the $-B_z$ events occurring near-midnight, we sort these data points by day of year and D_{st}. The results show that most of the events happen near summer solstice, some near winter solstice, and very few around the equinoxes. We then compare the D_{st} distributions when GOES is near midnight, and also when GOES is near midnight and measuring $-B_z$ values. The occurrence rate of $-B_z$ on the nightside is very low (<0.1%), and the distribution of D_{st} shows that these events happened preferentially during more stormy conditions. Finally, we examine the field geometry during these events by comparing the magnitudes of the total field and the Z component. For all the events, the total field magnitudes are much larger than the B_z values, which implies that the field lines are almost parallel to the equatorial plane. We found that GOES satellites do not observe large $-B_z$ fields at geosynchronous orbit as predicted by earlier models for a broad range of conditions.

[16] The weak $-B_z$ events observed by the GOES satellites near midnight are characterized by stretched field geometry and occur during stormy conditions with a tilted dipole. According to the schematic illustration of magnetic field lines during the solstices by *McPherron and Barfield* [1980], GOES could be in the lobe regions when measuring $-B_z$ near the midnight sector. Previous studies by *Thomsen et al.* [1994] and *Moldwin et al.* [1995] showed that GOES satellites were on open field lines in the magnetospheric lobe regions when $B_z < 0$, as shown by the extremely low ion fluxes at all energies (1 eV to 40 keV). *Fennell et al.* [1997] also showed near-Earth observations of the tail lobe and open field line regions from the particle dropout events observed by the Polar, HEO, and CRRES satellites.

[17] We conclude that the strong $-B_z$ at nightside near geosynchronous orbit, predicted by T96 and T02, is not a real effect, because its occurrence rate in our statistical study is very low (<0.1%). Rather, a possible explanation is that the earlier models assumed a linear dependence of the magnitude of the field sources on the external driving. The linear law breaks down once that driving gets extremely strong in comparison with average conditions. In the case of the September 25, 1998, event, the model inputs for 00:16 UT

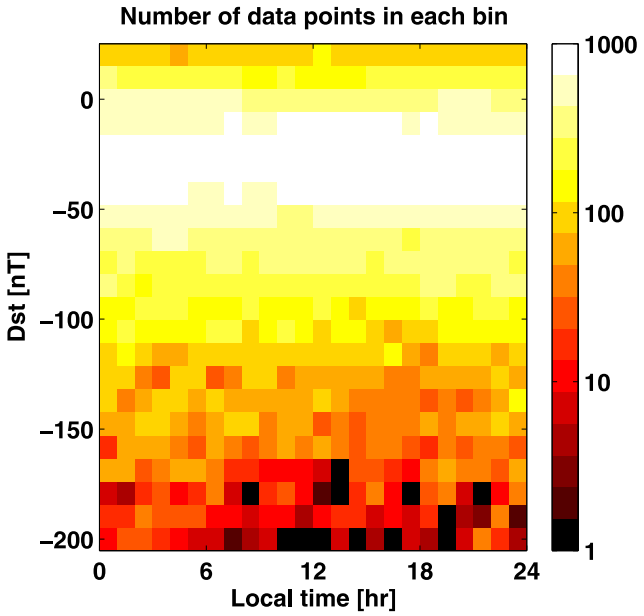

Figure 3. Local time and storm level distributions of the data points included in the statistical study.

are: P_{dyn} = 2 nPa, IMF B_z = −13 nT, and D_{st} = −205 nT. To determine if the strong $-B_z$ prediction is a recurrent problem in the models when reproducing other storm intervals, we repeat the comparisons between observations and models for additional storms.

5. Statistical Study for Tsyganenko Models During Major Storm Events

5.1. Storm-Time Data Distributions

[18] For the statistical study, we selected 52 major geomagnetic storms (D_{st} minimum ≤ −100 nT) from 1996 to 2004. These events must have continuous upstream solar wind data from either the ACE or Wind satellites and geosynchronous magnetic field data from the GOES satellites. During most of the storm intervals, there are magnetic field data from two GOES satellites which are located 4 hours apart in local time. For each storm event, data are taken from one day before the storm sudden commencement to after the recovery phase in order to include both storm and non-storm data.

[19] We run the Tsyganenko models with 5-min averaged D_{st} and solar wind data, which are time-shifted to the location of Earth. As described before, to confine the model validation to the magnetosphere, we exclude data that might have been collected outside the magnetopause in the following way. The GOES satellites measure $-B_z$ field when they are located beyond the dayside magnetopause during periods of southward IMF. Therefore data points that have $-B_z$ on the dayside (6–18 LT) are excluded from the study. These data represent 0.5% of the data set. Also, in order to get a meaningful result, we only include data from intervals when $D_{st} > -200$ nT to avoid examining the model for the most extreme cases that occurs less than 1% of the time.

[20] All the vector components of the magnetic field data and model outputs are converted to dipole magnetic coordinates [*Russell*, 1971]. Figure 3 shows the distribution of the 1.5×10^5 data points which satisfy the above criteria. In Figure 3, the horizontal axis is GOES local time bins in hours; the vertical axis is D_{st} levels from −200 to +20 nT with 10 nT step intervals. The pixel colors show the number of data points in each local time and D_{st} bin on a logarithmic scale. The number of data points has a maximum for $-40 < D_{st} \leq -30$ nT (>20,000 data points) and a minimum for $-200 < D_{st} \leq -190$ (~200 data points).

5.2. Maps of Model/Data Residual Fields

[21] Using the same format as Figure 3, we show the residual fields between the GOES data and model predictions ($\Delta B = B_{Data} - B_{Model}$) in Figure 4 to examine how

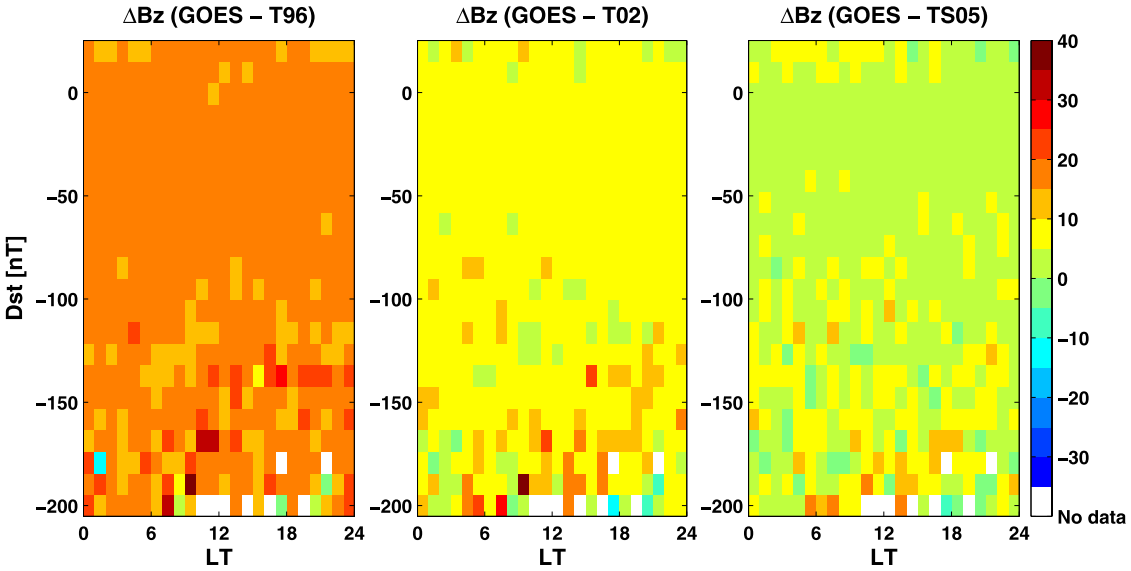

Figure 4. The residual fields (ΔB_z) between GOES data and Tsyganenko model outputs in different local time and D_{st} bins (T96, T02, and TS05, from left to right, respectively). The median data value is picked to represent all data points in each bin. The color scales of each panel are identical, from −35 to +40 nT. A white pixel marks a bin with no data.

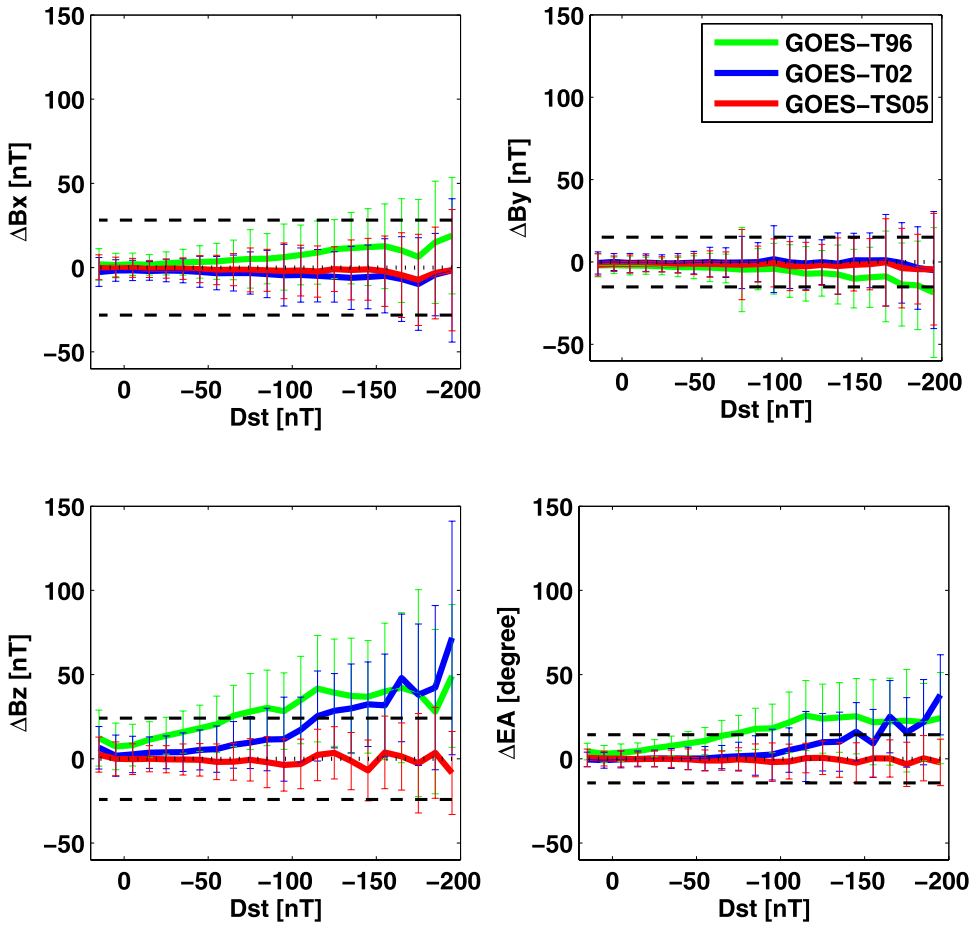

Figure 5. The residual fields between the GOES data and model predictions in vector components (B_x, B_y, and B_z) and elevation angle sorted by D_{st} bins. The thick color lines are results of individual models (T96, T02, and TS05 in green, blue, and red, respectively). The vertical error bars are the standard deviation of data in each bin.

well the Tsyganenko models reproduce geostationary fields at various D_{st} levels and local times. The median of the residual fields in each bin represents the difference between observations and model predictions. We plot the residual fields in the Z component with a color scale ranging from −35 to +40 nT. When the model underestimates (overestimates) the field, the pixel is red (blue). For a perfect model prediction, the pixel would be light green. A white pixel marks a bin with no data.

[22] T96 (left panel) underestimates geosynchronous B_z values (ΔB = 10∼20 nT, in orange) at most local times and D_{st} levels. T02 (center panel) also underestimates the field, but by a smaller value (ΔB = 5∼10 nT, in yellow). A recent statistical study by *Woodfield et al.* [2007] also shows a residual field of ∼20 nT in total magnetic field at ∼3 R_E by comparing T02 with Cluster data. TS05 (right panel) is the best predictor for most conditions (ΔB = 0∼5 nT, in light green). Generally, the models do best when D_{st} is greater than −50 nT. For strongly negative D_{st} levels, the current systems in the inner magnetosphere are very complicated and more difficult to predict. However, the latest TS05 model does well at reproducing the geostationary magnetic field even during strong storm conditions. This is possibly due to the fact that the fitted magnetic field data of this model contain GOES measurements. Nevertheless, the TS05 predictions do well not only for storm events that are included, but also for those storms not included in the data set.

5.3. Residual Fields in D_{st} and Local Time Bins

[23] To differentiate model performance as a function of D_{st} level and local time, the residual fields are sorted accordingly. Figures 5 and 6 show the residual fields between data and model outputs for vector components and elevation angle (EA) as a function of D_{st} (Figure 5) and local time (Figure 6). Elevation angle is defined such that 90 degrees (0 degrees) means the field line is perpendicular (parallel) to the dipole equatorial plane. The ΔB_x, ΔB_y, ΔB_z, ΔEA values of each model are shown with green, blue, and red lines, for T96, T02, and TS05, respectively. The error bars are the standard deviation of the data in each D_{st} or local time bin. The horizontal dashed lines are the standard deviation of data with small D_{st} values ($-20 \leq D_{st} \leq 0$) chosen to characterize the non−storm time magnetospheric variations at geosynchronous orbit. They are 28, 15, and 24 nT for the X, Y, and Z components, and 14 degrees for elevation angle. We use them to measure model performance against typical variations of the non-storm time magnetosphere.

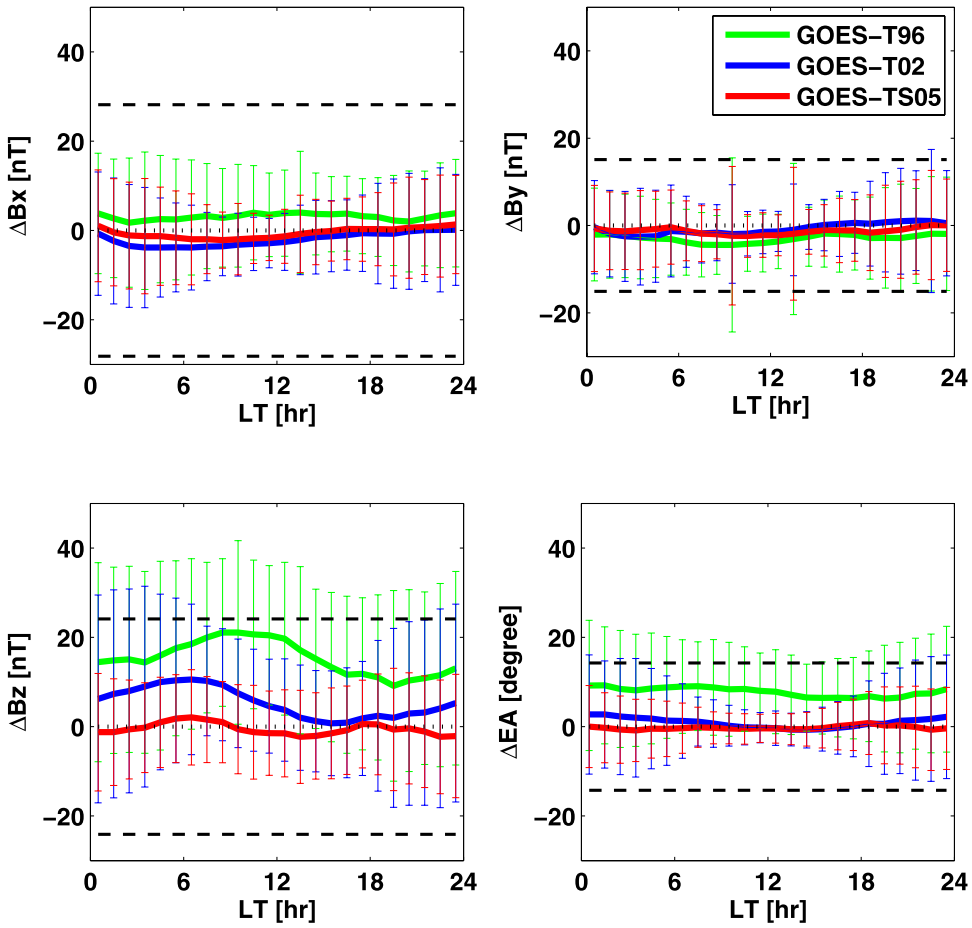

Figure 6. The residual fields between the GOES data and model predictions in vector components (B_x, B_y, and B_z) and elevation angle sorted by local time bins.

[24] In all conditions, the models predict the X and Y field components better than the Z component. The X and Y components are usually smaller and often less variable than the Z component so the difference between model and observation are also likely to be smaller. The D_{st} level plots show that the model performance becomes worse with increasing storm activity; this is especially true for T96 and T02 in the Z component. The underestimation of these two earlier models demonstrates that they include overly stretched field lines or unrealistic $-B_z$ predictions (like that during the Sep98 event). The unrealistic $-B_z$ prediction could be due to the earlier models being linearly dependent on the model inputs, while the response of the actual magnetosphere is non-linear. The local time plots show diurnal variations of the residual fields in the Z component. The earlier models predict smaller elevation angles compared to GOES data, which means the earlier model field lines are typically too stretched. At GOES local midnight, T96 and T02 model field lines are on average 2 and 10 degrees more tilted locally than is observed. In general, TS05 has the best prediction compared to the GOES data for all D_{st} levels and local times. In the ΔB_z versus D_{st} plot, the TS05 residual fields are always within the range of non-storm magnetospheric fluctuations, while the T96 and T02 residual fields exceed the range whenever D_{st} is smaller than -60 nT and -110 nT, respectively.

5.4. Residual Fields During Different Storm Phases

[25] The later Tsyganenko models (T02 and TS05) use solar wind and IMF data to represent the solar wind-magnetosphere coupling effects. However, the model inputs do not include the time evolution of D_{st} to represent the level of internal magnetospheric perturbations. During the storm main phase, D_{st} decreases in a matter of hours; during recovery phase, D_{st} increases over days. The same value of D_{st} can occur during both main and recovery phases; therefore, D_{st} alone cannot differentiate between the different magnetospheric states of the two different storm phases. To examine how well the models capture the field configurations for different times during storm evolution, we separate the data set into different storm phases, the storm main phase and the recovery phase; as well as pre-/post-storm intervals.

[26] We plot the residual B_z component between GOES data and model predictions for the different storm phases in Figure 7. The residual fields for the data points during the storm main phase are represented by circles (11% of all data), during the recovery phase by crosses (16%), and during the pre-/post-storm intervals by thick lines (73%). Three strong negative D_{st} levels in pre-/post-storm intervals are excluded from the study, because they do not have sufficient data.

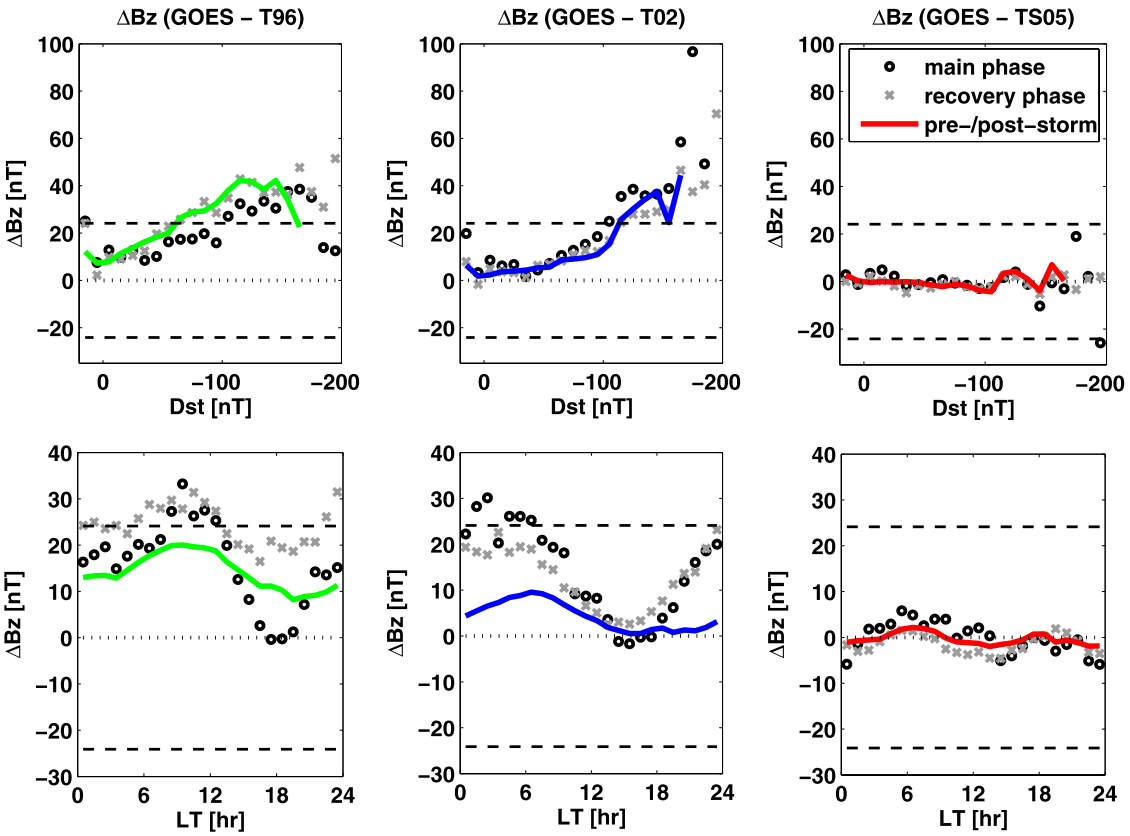

Figure 7. The residual B_z component between GOES data and model predictions for different storm phases: Storm main phase, early recovery phase, and the other intervals. The results of the T96, T02, and TS05 are on the left, center, right panels, respectively. The upper panels are the residual fields sorted by D_{st} level bins, and the lower panels are sorted by local time bins.

[27] The model performance during storm main and recovery phases is similar to that during the other time intervals for most D_{st} levels. However, the diurnal variations are stronger for storm main and recovery phases as opposed to the other non-storm intervals. This discrepancy is likely attributed to the effect of the less sophisticated model current systems present in the T96 and T02 models. Even though developed and optimized for storms, TS05 also reproduces the geostationary magnetic field very well for all levels of geomagnetic activity, including pre-/post-storm conditions. The field residuals between the GOES data and the TS05 outputs are small ($\leq$3 nT; <2% of the field magnitude) compared to the typical levels of variation of the non-storm magnetosphere ($\sim$24 nT).

6. Consequences of Field Model Errors: Radiation Belt Example

[28] Here we discuss the consequence of using field models for magnetospheric research, and quantify some effects of their errors. Global inaccuracies of magnetic field models could alter the results of related studies significantly, for example, inferred radial profiles of phase space density of radiation belt electrons [*Green and Kivelson*, 2004]. An imperfect field model affects the calculation of electron phase space density by inaccurately estimating K and L^*, the second and third adiabatic invariants, non-local parameters that require a field model. Next, we quantify how the discrepancies between different versions of the Tsyganenko models could affect radiation belt studies with a simple example.

[29] To estimate possible magnetic field mapping errors that could result from the models, we pick a time of moderate geomagnetic activity during the recovery phase of a magnetic storm, i.e., 5:00 UT on 16 May, 1997. Using the same inputs (P_{dyn} = 3 nPa, D_{st} = −39 nT, IMF B_y = −4 nT and B_z = 5.4 nT), all three models predict reasonable and similar field magnitudes at GOES-8 orbit, but each model predicts different field configurations, as shown in Figure 8. Although not shown in this figure, the model field lines traced from the location of GOES-8 [−6.25, 0, 2.1 R_E in GSM coordinates] to both hemispheres are rather different. More importantly, the predicted locations of the magnetic equator (B minimum point) differ considerably. Figure 8a shows that T96 and T02 field lines are more stretched than those of TS05. Their B minimum points are 0.8 and 0.3 R_E further from TS05's prediction.

[30] We also compare in Figure 8b how electron pitch angles measured at GOES-8 map in a model-dependent way to the magnetic equator. If we assume that GOES-8 measures electrons with pitch angles ranging from 0 to 90 degrees (horizontal axis), then we calculate the pitch angle at the magnetic equator (vertical axis) using different models. The results imply a great difference in mapping particle distributions when utilizing different field models. The local off-equatorial particles map to smaller pitch

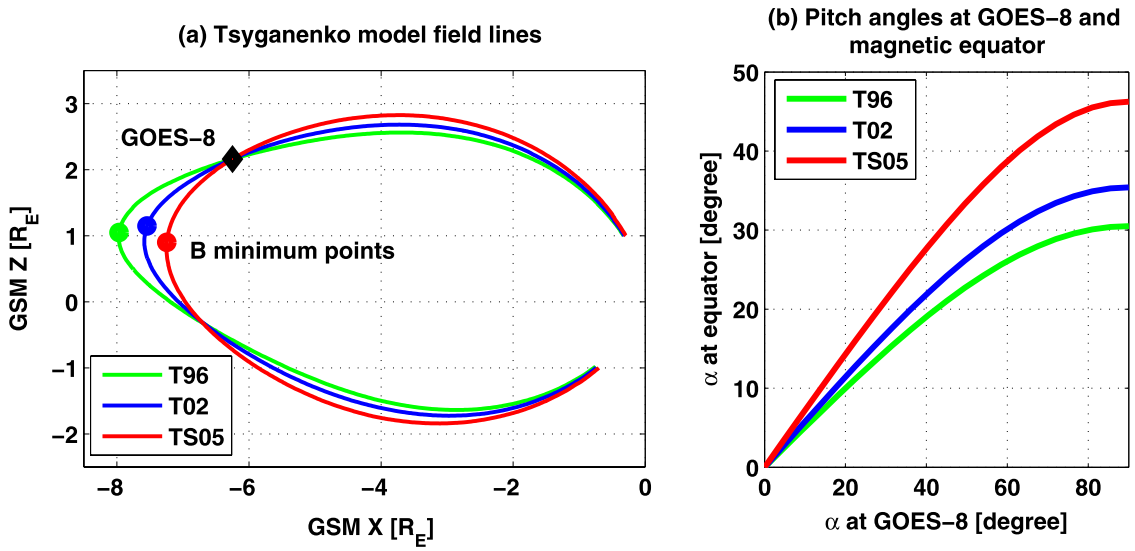

Figure 8. Discrepancies between Tsyganenko models using same inputs for 16 May 1997, 5 UT: (a) model field lines traced from GOES-8's position; (b) pitch angles at GOES-8's position and at magnetic equator (B minimum point).

angles at the magnetic equator. This effect is largest for the locally mirroring particles (90 degrees pitch angle). TS05 (T96) predicts that locally mirroring particles at GOES-8 position map to 45 (30) degrees pitch angle at the magnetic equator. When interpreting electron observations off the magnetic equator (GOES−8 at ∼10 degrees north of magnetic equator), even only 15 degrees uncertainty in pitch angle can lead to misinterpretations in analysis of radiation belt electron distributions.

[31] Finally, we estimate the L^* values at a fixed point in space to demonstrate the effect of using different field models. L^* depends inversely on Φ, the total magnetic flux enclosed by the drift orbit of an electron [*Roederer*, 1970]. We calculate the L^* values following the methodology of *Roederer* [1970]: (i) follow a particle trajectory in the equatorial plane; (ii) trace the field lines which thread the particle's trajectory to Earth's surface; and (iii) integrate the magnetic flux over the area defined by the mapped trajectory at Earth's surface. From the same initial point at geosynchronous orbit at midnight [−6.6, 0, 0 R_E], the L^* values estimated by T96, T02, and TS05 models are 5.2, 5.6, and 6.0, respectively. These models predict similar particle trajectories at the equatorial plane. However, the earlier models have more stretched field lines that connect to lower latitude at Earth's surface which lead to smaller L^* values. Again, this example demonstrates that small deviations between field models have a significant influence on the model-dependent invariants used to interpret radiation belt electrons (e.g., L^* varies by ∼13% between T96 and TS05 at geosynchronous orbit).

7. Conclusions

[32] We evaluate the three most recent Tsyganenko models (T96, T02, and TS05) during magnetic storms by quantitatively comparing the model outputs with the observed geostationary magnetic field. Input values exceeding the earlier models' (T96 and T02) limits tend to overdrive the models during a major storm, causing them to predict anomalous, strong $-B_z$ values at GOES near midnight. The results of a broad GOES data survey show no such sign of this strong $-B_z$ predicted by those two models. Finally, we quantify the performance of each model by comparing to the typical non-storm time magnetospheric variations at geosynchronous orbit for each vector component and magnetic elevation angle.

[33] The comparisons of GOES data and model predictions during the Sep98 event show the relative importance of each model current component throughout a magnetic storm. T96 has overly strong tail and ring currents, and T02 overestimates the tail current during the storm main phase, thus predicting strong $-B_z$ fields at GOES orbit. The statistical study shows the accuracy and limitations of each model at different local times and for various geomagnetic activity levels. The average model predictions for the B_x and B_y components are within the typical range of magnetospheric variations in all cases. However, B_z predictions of T96 and T02 exceed the fluctuation range when D_{st} is smaller than −60 and −110 nT, respectively. Except for TS05, even when the models are within their prescribed limits, they are too stretched in the vicinity of geosynchronous orbit. To examine the models at similar D_{st} values but different stages of the D_{st} time evolutions (+versus− $\frac{dD_{st}}{dt}$), we separated the data into different storm phases. TS05 predicts the geostationary field best for all conditions, while the earlier models have larger errors during the storm main and recovery phases.

[34] The performance of databased models depends heavily on the data set that is used to fit the model coefficients. The earlier models (T96 and T02) use both storm and non-storm time data. However, storm time data is only a few percent of the data set. Consequently, these models are adequate for predicting the quiet time magnetosphere, but not stormy conditions. On the other hand, TS05 uses 37 magnetic storm events for its data set. This improvement makes the new model efficient at reproducing

storm-time field magnitudes and configurations, even during strong storm activity. In addition, both the time-integration effects and the non-linear interpolation of the current calculation limit the growth of the field sources during active conditions, and thus avoid problems evident in the earlier models (e.g., anomalous $-B_z$ at GOES near midnight). Even though it is constructed from sparse satellite data in time and space, TS05 describes the storm-time field configuration of the inner magnetosphere with impressive success. Nevertheless, outside the model spatial domain and during extreme conditions, model users should use it with caution.

[35] **Acknowledgments.** We would like to thank E. L. Kepko, W. J. Hughes, A. P. Jordan, and E. E. Wilson for helpful discussions and suggestions. This material is based upon work supported by Center for Integrated Space Weather Modeling (CISM), which is funded by the Science and Technology Centers Program of the National Science Foundation under agreement ATM-0120950.

[36] Amitava Bhattacharjee thanks Robert V. Hilmer and another reviewer for their assistance in evaluating this paper.

References

Fennell, J. F., J. B. Blake, J. L. Roeder, R. Sheldon, and H. E. Spence (1997), Tail lobe and open field line region entries at mid to high latitudes, *Adv. Space Res.*, *20*(3), 431–435.

Green, J. C., and M. G. Kivelson (2004), Relativistic electrons in the outer radiation belt: Differentiating between acceleration mechanisms, *J. Geophys. Res.*, *109*, A03213, doi:10.1029/2003JA010153.

Hones, E. W. (1963), Motions of charged particles trapped in the Earth's magnetosphere, *J. Geophys. Res.*, *68*, 1209.

Huang, C.-L., H. E. Spence, J. G. Lyon, F. R. Toffoletto, H. J. Singer, and S. Sazykin (2006), Storm-time configuration of the inner magnetosphere: Lyon-Fedder-Mobarry MHD code, Tsyganenko model, and GOES observations, *J. Geophys. Res.*, *111*, A11516, doi:10.1029/2006JA011626.

McPherron, R. L., and J. N. Barfield (1980), A seasonal change in the effect of field-aligned currents at synchronous orbit, *J. Geophys. Res.*, *85*, 6743–6746.

Mead, G. D. (1964), Deformation of the geomagnetic field by the solar wind, *J. Geophys. Res.*, *69*, 1181.

Mead, G. D., and D. H. Fairfield (1975), A quantitative magnetospheric model derived from spacecraft magnetometer data, *J. Geophys. Res.*, *80*, 523–534.

Moldwin, M. B., M. F. Thomsen, S. J. Bame, D. J. McComas, J. Birn, G. D. Reeves, R. Nemzek, and R. D. Belian (1995), Flux dropouts of plasma and energetic particles at geosynchronous orbit during large geomagnetic storms: Entry into the lobes, *J. Geophys. Res.*, *100*, 8031–8043.

Olson, W. P., and A. K. Pfitzer (1974), A quantitative model of the magnetospheric magnetic field, *J. Geophys. Res.*, *79*, 3739–3748.

Olson, W. P., and K. A. Pfitzer (1977), Magnetospheric magnetic field modeling, in *Annual Scientific Report*, AFOSR, contract No. F44620-C-0033.

Peredo, M., D. P. Stern, and N. A. Tsyganenko (1993), Are existing magnetospheric models excessively stretched?, *J. Geophys. Res.*, *98*, 15343–15354.

Pulkkinen, T. I., and N. A. Tsyganenko (1996), Testing the accuracy of magnetospheric model field line mapping, *J. Geophys. Res.*, *101*, 27431–27442.

Pulkkinen, T. I., D. N. Baker, R. J. Walker, J. Reader, and M. Ashour-Abdalla (1995), Comparison of empirical magnetic field models and global MHD simulations: The near-tail currents, *Geophys. Res. Lett.*, *22*, 675–678.

Reeves, G. D., L. A. Weiss, M. F. Thomsen, and D. J. McComas (1996), A quantitative test of different magnetic field models using conjunctions between DMSP and geosynchronous orbit, in *Radiation Belt Models and Standards*, vol. 97, edited by J. F. Lemaire, D. Heynderickx, and D. N. Baker, pp. 167–172, AGU, Washington, D.C.

Roederer, J. G. (1970), *Dynamics of Geomagnetically Trapped Radiation*, Springer, New York.

Russell, C. T. (1971), Geophysical coordinate transformation, *Cosmic Electrodyn.*, *2*, 184–196.

Shue, J.-H., et al. (1998), Magnetopause location under extreme solar wind conditions, *J. Geophys. Res.*, *103*, 17691–17700.

Sibeck, D. G., R. E. Lopez, and E. C. Roelof (1991), Solar wind control of the magnetopause shape, location, and motion, *J. Geophys. Res.*, *96*, 5489–5495.

Spence, H. E., M. G. Kivelson, and R. J. Walker (1987), Static magnetic field models consistent with nearly isotropic plasma pressure, *Geophys. Res. Lett.*, *14*, 872–875.

Stern, D. P. (1994), The art of mapping the magnetosphere, *J. Geophys. Res.*, *99*, 17,169–17,198.

Taylor, H. E., and E. W. Hones (1965), Adiabatic motion of auroral particles in a model of the electric and magnetic fields surrounding the Earth, *J. Geophys. Res.*, *70*, 3605.

Thomsen, M. E., S. J. Bame, D. J. McComas, M. B. Moldwin, and F. R. Moore (1994), The magnetospheric lobe at geosynchronous orbit, *J. Geophys. Res.*, *99*, 17283–17293.

Thomsen, M. F., D. J. McComas, G. D. Reeves, and L. A. Weiss (1996), An observational test of the Tsyganenko (T89a) model of the magnetospheric field, *J. Geophys. Res.*, *101*, 24827–24836.

Tsyganenko, N. A., and A. V. Usmanov (1982), Determination of the magnetospheric current system parameters and development of experimental geomagnetic field models based on data from IMP and HEOS satellites, *Planet. Space Sci.*, *30*(10), 985–998.

Tsyganenko, N. A. (1987), Global quantitative models of the geomagnetic field in the cislunar magnetosphere for different disturbance levels, *Planet. Space Sci.*, *35*, 1347–1358.

Tsyganenko, N. A. (1989), A magnetospheric magnetic field model with a warped tail current sheet, *Planet. Space Sci.*, *37*, 5–20.

Tsyganenko, N. A. (1995), Modeling the Earth's magnetospheric magnetic field confined within a realistic magnetopause, *J. Geophys. Res.*, *100*, 5599.

Tsyganenko, N. A. (1996), Effects of the solar wind conditions on the global magnetospheric configuration as deduced from data-based field models, in *European Space Agency Publication*, ESA SP-389, pp. 181–185.

Tsyganenko, N. A. (2002a), A model of the near magnetosphere with a dawn-dusk asymmetry, 1, Mathematical structure, *J. Geophys. Res.*, *107*(A8), 1179, doi:10.1029/2001JA000219.

Tsyganenko, N. A. (2002b), A model of the near magnetosphere with a dawn-dusk asymmetry, 2, Parameterization and fitting to observations, *J. Geophys. Res.*, *107*(A8), 1176, doi:10.1029/2001JA000220.

Tsyganenko, N. A., and M. I. Sitnov (2005), Modeling the dynamics of the inner magnetosphere during strong geomagnetic storms, *J. Geophys. Res.*, *110*, A03208, doi:10.1029/2004JA010798.

Tsyganenko, N. A., H. J. Singer, and J. C. Kasper (2003), Storm-time distortion of the inner magnetosphere: How severe can it get?, *J. Geophys. Res.*, *108*(A5), 1209, doi:10.1029/2002JA009808.

Ukhorskiy, A. Y., B. J. Anderson, K. Takahashi, and N. A. Tsyganenko (2006), Impact of ULF oscillations in solar wind dynamic pressure on the outer radiation belt electrons, *Geophys. Res. Lett.*, *33*, L06111, doi:10.1029/2005GL024380.

Walker, R. J. (1976), An evaluation of recent quantitative magnetospheric magnetic field models, *Rev. Geophys. Space Phys.*, *14*, 411–427.

Williams, D. J., and G. D. Mead (1965), Nightside magnetosphere configuration as obtained from trapped electrons at 1100 kilometers, *J. Geophys. Res.*, *70*, 3017.

Woodfield, E. E., M. W. Dunlop, R. Holme, J. A. Davies, and M. A. Hapgood (2007), A comparison of cluster magnetic data with the Tsyganenko 2001 model, *J. Geophys. Res.*, *112*, A06248, doi:10.1029/2006JA012217.

C.-L. Huang and H. E. Spence, Center for Space Physics, Boston University, 725 Commonwealth Avenue, Room 506, Boston, MA 02215, USA. (hcl@bu.edu)

H. J. Singer, Space Weather Prediction Center, NOAA, 325 Broadway, Boulder, CO 80305, USA.

N. A. Tsyganenko, Department of Terrestrial Physics, Institute of Physics, University of Saint-Petersburg, Petrodvorets, Saint-Petersburg 198504, Russian Federation.